INTERNATIONAL JOURNAL FOR NUMERICAL METHODS IN FLUIDS
Int. J. Numer. Meth. Fluids 2007; **53**:1755–1775
Published online 25 October 2006 in Wiley InterScience (www.interscience.wiley.com). DOI: 10.1002/fld.1383

A numerical method for flows in porous and homogenous fluid domains coupled at the interface by stress jump

P. Yu[1,*,†], T. S. Lee[1,‡], Y. Zeng[1] and H. T. Low[2,‡]

[1]*Department of Mechanical Engineering, National University of Singapore, Singapore 117576, Singapore*
[2]*Division of Bioengineering, National University of Singapore, Singapore 117576, Singapore*

SUMMARY

A numerical method was developed for flows involving an interface between a homogenous fluid and a porous medium. The numerical method is based on the finite volume method with body-fitted and multi-block grids. A generalized model, which includes Brinkman term, Forcheimmer term and non-linear convective term, was used to govern the flow in the porous medium region. At its interface, a shear stress jump that includes the inertial effect was imposed, together with a continuity of normal stress. Furthermore, the effect of the jump condition on the diffusive flux was considered, additional to that on the convective part which has been usually considered. Numerical results of three flow configurations are presented. The method is suitable for coupled problems with regions of homogeneous fluid and porous medium, which have complex geometries. Copyright © 2006 John Wiley & Sons, Ltd.

Received 1 March 2006; Revised 28 August 2006; Accepted 1 September 2006

KEY WORDS: interfacial condition; stress jump; porous medium; block-structured grids

1. INTRODUCTION

The study of flow systems which compose of a porous medium and a homogenous fluid has attracted much attention since they occur in a wide range of the industrial and environmental applications. Examples of practical applications are: flow past porous scaffolds in bioreactors, drying process, electronic cooling, ceramic processing, overland flow during rainfall and ground-water pollution. Two different approaches, the single-domain approach [1, 2] and the two-domain approach [3, 4], are usually used to solve this type of problems.

In the single-domain approach, the composite region is considered as a continuum and one set of general governing equations is applied for the whole domain. The explicit formulation of

*Correspondence to: P. Yu, Department of Mechanical Engineering, National University of Singapore, Singapore 117576, Singapore.
†E-mail: g0202355@nus.edu.sg
‡Associate Professor.

Table I. Interface boundary conditions between porous medium and homogenous fluid domains.

Model	Velocity	Velocity gradient	Reference
1		$\left.\frac{\partial u_x}{\partial y}\right\|_{\text{fluid}} = \frac{\alpha}{\sqrt{K}}(u_x\|_{\text{interface}} - \langle u\rangle_\infty)$	[7]
2	$\langle u\rangle_x\|_{\text{porous}} = u_x\|_{\text{fluid}}$	$\left.\frac{\partial\langle u\rangle_x}{\partial y}\right\|_{\text{porous}} = \left.\frac{\partial u_x}{\partial y}\right\|_{\text{fluid}}$	[8, 9]
3	$\langle u\rangle_x\|_{\text{porous}} = u_x\|_{\text{fluid}}$	$\mu_{\text{eff}}\left.\frac{\partial\langle u\rangle_x}{\partial y}\right\|_{\text{porous}} = \mu\left.\frac{\partial u_x}{\partial y}\right\|_{\text{fluid}}$	[10]
4	$\langle u\rangle_x\|_{\text{porous}} = u_x\|_{\text{fluid}}$	$\frac{\mu}{\varepsilon}\left.\frac{\partial\langle u\rangle_x}{\partial y}\right\|_{\text{porous}} - \mu\left.\frac{\partial u_x}{\partial y}\right\|_{\text{fluid}} = \beta\left.\frac{\mu}{\sqrt{K}}u_x\right\|_{\text{interface}}$	[11, 12]
5	$\langle u\rangle_x\|_{\text{porous}} = u_x\|_{\text{fluid}}$	$\frac{\mu}{\varepsilon}\left.\frac{\partial\langle u\rangle_x}{\partial y}\right\|_{\text{porous}} - \mu\left.\frac{\partial u_x}{\partial y}\right\|_{\text{fluid}} = \beta\left.\frac{\mu}{\sqrt{K}}u_x\right\|_{\text{interface}} + \beta_1\rho u_x^2\|_{\text{interface}}$	[13]

boundary conditions is avoided at the interface and the transitions of the properties between the fluid and porous medium are achieved by certain artefacts [5]. Although this method is relatively easier to implement, the flow behaviour at the interface may not be simulated properly, depending on how the code is structured [6].

In the two-domain approach, two sets of governing equations are applied to describe the flow in the two regions and additional boundary conditions are applied at the interface to close the two sets of equations. This method is more reliable since it tries to simulate the flow behaviour at the interface. Hence, in the present study, the two-domain approach, with the implementation of the interface boundary conditions, is considered. A list of proposed boundary conditions at the porous–fluid interface is summarized in Table I.

One of the several early studies on the interface boundary conditions is that by Beavers and Joseph [7]. In their approach, the flows in a homogenous fluid and a porous medium are governed by the Navier–Stokes and Darcy equations, respectively. A semi-empirical slip boundary condition was proposed at the interface, because the flows in the different regions are governed by the corresponding partial differential equations of different orders. To make the governing equations of the same order, Neale and Nader [8] introduced a Brinkman term in the Darcy equation for the porous medium; and thus, proposed continuous boundary conditions in both stress and velocity. By matching both velocity and stress, Vafai and Kim [9] provided an exact solution for the fluid flow at the interface, which includes the inertial and boundary effects. In an alternative model [10], the effective viscosity was used in the formulation of the continuous stress condition at the interface.

A stress jump condition at the interface was deduced by Ochoa-Tapia and Whitaker [11, 12] based on the non-local form of the volume-averaged method. Based on the Forchheimer equation with the Brinkman correction and the Navier–Stokes Equation, Ochoa-Tapia and Whitaker [13]

DOI: 10.1002/fld

developed another stress jump condition which includes the inertial effects. Two coefficients appear in this jump condition: one is associated with an excess viscous stress and the other is related to an excess inertial stress.

Numerical solutions for the coupled viscous and porous flows have been attempted by many researchers [2–4, 14, 15]. Jue [2] simulated vortex shedding behind a porous square cylinder by finite element method. In his study, a general non-Darcy porous media model was applied to describe the flows both inside and outside the cylinder. A harmonic mean was used to treat the sudden change between the fluid and porous medium. Costa *et al*. [4] proposed a control-volume finite element method to simulate the problems of coupled viscous and porous flows. A continuity of both velocity and stress at the interface was assumed and no special or additional procedure was needed to impose the interfacial boundary conditions. Betchen *et al*. [15] developed a finite volume model, also based on continuity of both velocity and stress, but special attention was given to the pressure–velocity coupling at the interface.

Different types of interfacial conditions between a porous medium and a homogenous fluid have been proposed; and found to have a pronounced effect on the velocity field as shown by Alazmi and Vafai [16]. Although the one-domain approach, or a continuity of both velocity and stress, is easier to implement, the stress jump conditions have been adopted by researchers.

The implementation of the numerical methodology on the stress jump condition based on Ochoa-Tapia and Whitaker [11, 12] can be found in the work of Silva and de Lemos [3]. Although they proposed that their treatment could be used in a complex geometry, their results were based on finite volume method in an orthogonal Cartesian coordinate system and for the case of fully developed flow. In their study, only the jump in shear stress was included and no special treatment on velocity derivatives was mentioned. However, for flow in general, it is needed to consider how to formulate the velocity derivatives at the interface. Also, for the two-dimensional problem, the normal stress condition is needed to close the sets of equations.

The objective of the present study was to develop a numerical method based on finite volume method with a collocated variable arrangement to treat the stress jump condition given by Ochoa-Tapia and Whitaker [13], which includes the inertial effects. As the interface naturally divides the whole domain into different parts and its location is known *a priori*, the multi-block method is used. By combining body-fitted and multi-block grids, the present method is effective for the coupled problem in the homogeneous fluid and porous medium regions with complex geometries.

2. GOVERNING EQUATIONS AND BOUNDARY CONDITIONS

Considering steady, laminar flow of an incompressible, viscous fluid, the governing equations for a homogenous fluid region, using vector form, can be written as

$$\nabla \cdot \mathbf{u} = 0 \tag{1}$$

$$\nabla \cdot (\rho \mathbf{u}\mathbf{u}) = -\nabla p + \mu \nabla^2 \mathbf{u} \tag{2}$$

where p is the pressure, ρ is the mass density of the fluid and μ is the fluid dynamic viscosity.

The porous medium is considered to be rigid, homogeneous and isotropic; and saturated with the same single-phase fluid as that in the homogenous fluid region. Considering viscous and

DOI: 10.1002/fld

inertial effects, the governing equations for porous region based on Darcy–Brinkman–Forchheimer extended model can be expressed as [17, 18]

$$\nabla \cdot \mathbf{u} = 0 \tag{3}$$

$$\underbrace{\nabla \cdot \left(\frac{\rho \mathbf{u}\mathbf{u}}{\varepsilon}\right)}_{\text{Convective Term}} = - \underbrace{\nabla(\varepsilon p^*)}_{\text{Pressure Term}} + \underbrace{\mu \nabla^2 \mathbf{u}}_{\text{Brinkman Term}} - \underbrace{\frac{\mu \varepsilon}{K}\mathbf{u}}_{\text{Darcy Term}} - \underbrace{\frac{\rho \varepsilon C_{\mathrm{F}} |\mathbf{u}|}{\sqrt{K}}\mathbf{u}}_{\text{Forchheimer Term}} \tag{4}$$

where $\mathbf{u}$ is the local average velocity vector (Darcy velocity), p^* is the intrinsic average pressure, μ is the fluid dynamic viscosity, ε is the porosity, K is the permeability and C_{F} is Forchheimer coefficient. Note that throughout the paper, viscosity means dynamic viscosity of the fluid but not the effective (Brinkman) viscosity. The '*' denotes the intrinsic average. The local average and intrinsic average can be linked by the Dupuit–Forchheimer relationship, for example, $p = \varepsilon p^*$.

At the interface between the homogeneous fluid and porous medium regions, additional boundary conditions must be applied to couple the flows in the two regions. In the present study, the stress jump condition [13] is applied

$$\frac{\mu}{\varepsilon}\frac{\partial u_t}{\partial n}\bigg|_{\text{porous}} - \mu \frac{\partial u_t}{\partial n}\bigg|_{\text{fluid}} = \beta \frac{\mu}{\sqrt{K}} u_t \bigg|_{\text{interface}} + \beta_1 \rho u_t^2 \tag{5}$$

where in the porous medium region, u_t is the Darcy velocity component parallel to the interface aligned with the direction t and normal to the direction n while in the homogenous fluid region u_t is the fluid velocity component parallel to the interface; β and β_1 are adjustable parameters which account for the stress jump at the interface.

Ochoa-Tapia and Whitaker [13] derived analytical expressions for parameters β and β_1 which indicate their dependence on permeability and porosity. They concluded that these two parameters are both of order one. Ochoa-Tapia and Whitaker [12] experimentally determined that β varies from $+0.7$ to -1.0 for different materials with permeability varying from 15×10^{-6} to 127×10^{-6} in^2 and average pore size from 0.016 to 0.045 in. There is presently no experimental data for β_1. It is not known how much the two parameters may change from one type of interface to another; and it is assumed in this study that the changes should be in the same range as those for different types of materials. Thus, for the purpose of demonstrating the implementation of the present formulation, both β and β_1 are varied in the range -0.7 to $+0.7$ in the present study.

In addition to Equation (5), the continuity of velocity and normal stress prevailing at the interface is given by

$$\mathbf{u}|_{\text{fluid}} = \mathbf{u}|_{\text{porous}} = \mathbf{v}_{\text{interface}} \tag{6}$$

$$\frac{\mu}{\varepsilon}\frac{\partial u_n}{\partial n}\bigg|_{\text{porous}} - \mu \frac{\partial u_n}{\partial n}\bigg|_{\text{fluid}} = 0 \tag{7}$$

where in the porous medium region, u_n is the Darcy velocity component normal to the interface and in the homogenous fluid region, u_n is the fluid velocity component normal to the interface. By combining with the appropriate boundary conditions of the composite region, Equations (1)–(7) can be used to simulate the flow in a system composed of a porous medium and a homogenous fluid.

DOI: 10.1002/fld

3. DISCRETIZATION

3.1. Homogenous fluid region

A typical control volume is shown in Figure 1. For a general dependent variable φ, a final discrete form over the control volume can be written as

$$F_e + F_w + F_n + F_s = S \tag{8}$$

where F_e, F_w, F_n and F_s are the overall fluxes (including both convection and diffusion) of φ at faces e, w, n, s, which denote *east*, *west*, *north*, and *south* of the control volume and S is the source term. The detailed numerical methodology for obtaining the convective flux (F_e^c, F_w^c, F_n^c and F_s^c) and diffusive flux (F_e^d, F_w^d, F_n^d and F_s^d) are given by Ferziger and Perić [19].

With the midpoint rule approximation, the convective flux at face *east* can be calculated as

$$F_e^c = \int_{S_e} \rho\varphi\mathbf{u}\cdot\mathbf{n}\,\mathrm{d}S \approx m_e\varphi_e \tag{9}$$

where m_e is the mass flux cross the surface e, S_e is the surface area of face e and φ_e is the value of φ at the centre of the cell face. m_e and S_e can be calculated as

$$m_e = \rho_e(S^x u + S^y v)_e, \quad S_e = \sqrt{(S_e^x)^2 + (S_e^y)^2} \tag{10}$$

where u and v are the velocity components in the x and y directions, S^x and S^y are the surface vector components.

To avoid the non-orthogonal effect, the midpoint rule with the deferred correction term [20] applied to the integrated diffusive flux is given by

$$F_e^d = \mu_e\left(\frac{\partial\varphi}{\partial n}\right)_e S_e = \mu_e S_e\left(\frac{\partial\varphi}{\partial\xi}\right)_e + \mu_e S_e\left[\overline{\left(\frac{\partial\varphi}{\partial n}\right)_e} - \overline{\left(\frac{\partial\varphi}{\partial\xi}\right)_e}\right]^{\mathrm{old}} \tag{11}$$

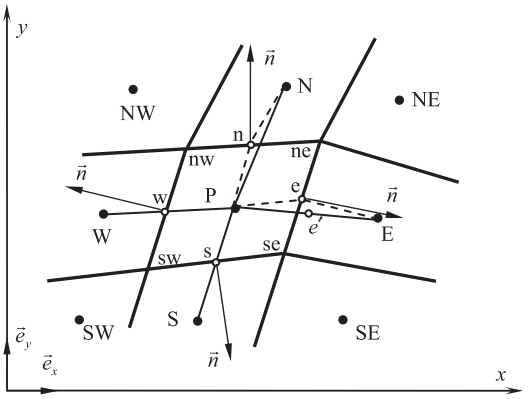

Figure 1. A typical two-dimensional control volume.

DOI: 10.1002/fld

If an implicit flux approximation of the term $(\partial\varphi/\partial\xi)_e$ is applied, the final expression of Equation (11) then becomes

$$F_e^d = \mu_e S_e \frac{\varphi_E - \varphi_P}{L_{PE}} + \mu_e S_e \overline{(\text{grad}\,\varphi)_e}^{\text{old}} \cdot (\mathbf{n} - \mathbf{i}_\xi) \tag{12}$$

where L_{PE} stands for the distance between P and E, $\mathbf{i}_\xi$ is the unit vector in the ξ-direction.

The different methods to approximate the value of φ and its derivative at the cell face result in different interpolation schemes. In the present study, the central difference scheme (CDS) is used. Then the cell-face values of the variables are approximated as

$$\varphi_e \approx \varphi_{e'} = \lambda_e \varphi_E + (1 - \lambda_e)\varphi_P \quad \text{for face e} \tag{13}$$

where the interpolation factor λ_e is defined as

$$\lambda_e = \frac{|\mathbf{r}_e - \mathbf{r}_P|}{|\mathbf{r}_e - \mathbf{r}_P| + |\mathbf{r}_E - \mathbf{r}_e|} \tag{14}$$

where $\mathbf{r}_e$ is the position vector.

Equation (13) is a second-order approximation at the location e′ on the straight line connecting nodes P and E (Figure 1). If the cell-face centre e does not coincide with the location e′, a correction term needs to be added in Equation (13) to restore the second-order accuracy, which can be expressed as follows:

$$\varphi_e \approx \varphi_{e'} + (\text{grad}\,\varphi)_{e'} \cdot (\mathbf{r}_e - \mathbf{r}_{e'}) \tag{15}$$

To obtain the deferred derivatives at the cell face, they are calculated first at the control volume centres and then interpolated to the cell faces. By using the Gauss' theorem, the derivative at the control volume (CV) centres can be approximated by the average value over the cell

$$\left(\frac{\partial\varphi}{\partial x_i}\right)_P \approx \frac{\int_\Omega \frac{\partial\varphi}{\partial x_i}\,d\Omega}{\Delta\Omega} = \int_S \varphi \mathbf{i}_i \cdot \mathbf{n}\,dS \approx \sum_c \varphi_c S_c^i, \quad c = e, n, w, s \tag{16}$$

Then the cell-centre derivatives can also be interpolated to the cell-face centres using the same interpolation as that described by Equations (13)–(15).

The volume integral of the source term is

$$Q_\varphi = \int_\Omega S_\varphi\,d\Omega \approx S_\varphi \Delta\Omega \tag{17}$$

where Ω is the cell volume.

The momentum equations contain a contribution from the pressure. The volume integral of the pressure gradient term in u-momentum equation can be obtained by

$$Q_{u,P}^p = \int_\Omega -\left(\frac{\partial p}{\partial x}\right)_P d\Omega \approx -\left(\frac{\delta p}{\delta x}\right)_P \Delta\Omega \tag{18}$$

Then the final discrete form of the u-momentum equation is

$$A_P^u u_P + \sum_l A_l^u u_l = Q_{u,P}^* - \left(\frac{\delta p}{\delta x}\right)_P \Delta\Omega \tag{19}$$

DOI: 10.1002/fld

where P is the index of an arbitrary node, the index l denotes the four neighbouring points E, W, S, N, the coefficients A_{P}^{φ}, A_{E}^{φ}, A_{W}^{φ}, A_{N}^{φ}, A_{S}^{φ} are those of the resultant algebraic equations and $Q_{u,P}^{*}$ is the integral of the source term contributed by other forces.

In the present study, SIMPLEC method [21] is applied to couple the velocity and pressure. To avoid oscillations in the pressure or velocity, the interpolation proposed by Rhie and Chow [22] is adopted

$$u_{\mathrm{e}}^{m}=\overline{(u^{m})_{\mathrm{e}}}-\Delta\Omega_{\mathrm{e}}\overline{\left(\frac{1}{A_{P}^{u}+\sum_{l}A_{l}^{u}}\right)_{\mathrm{e}}}\left[\left(\frac{\delta p}{\delta x}\right)_{\mathrm{e}}-\overline{\left(\frac{\delta p}{\delta x}\right)_{\mathrm{e}}}\right]^{m-1} \tag{20}$$

3.2. Porous medium region

Equations (3) and (4) recover the standard Navier–Stokes equations when the porosity approaches unity. Thus, the discretizing procedure for porous medium is similar to that for the homogenous fluid as the two sets of governing equations are similar in form. The discretized diffusion flux is similar in form to Equation (12). The convective flux at a cell face is similar in form to Equation (9) except for a small change

$$F_{\mathrm{e}}^{\mathrm{c}}=\int_{S_{\mathrm{e}}}\frac{\rho u}{\varepsilon}\,\mathbf{u}\cdot\mathbf{n}\,\mathrm{d}S\approx m_{\mathrm{e}}u_{\mathrm{e}}/\varepsilon_{\mathrm{e}} \tag{21}$$

The volume integral of the pressure gradient term (similar in form to Equation (18)) is

$$Q_{u,P}^{p*}=\int_{\Omega}-\left(\frac{\partial(\varepsilon p^{*})}{\partial x}\right)_{P}\mathrm{d}\Omega\approx-\left(\varepsilon\frac{\delta p}{\delta x}\right)_{P}\Delta\Omega \tag{22}$$

For the Darcy term in Equation (4), the volume integral can be expressed as

$$Q_{\mathrm{D}}^{u}=\int_{\Omega}-\left(\frac{\mu\varepsilon}{K}u\right)_{p}\mathrm{d}\Omega=-\left(\frac{\mu\varepsilon}{K}\right)_{p}\Delta\Omega\cdot u_{p} \tag{23}$$

For the Forchheimer term, the volume integral is given by

$$Q_{\mathrm{F}}^{u}=\int_{\Omega}-\left(\frac{\rho\varepsilon C_{\mathrm{F}}\sqrt{u^{2}+v^{2}}}{\sqrt{K}}u\right)_{p}\mathrm{d}\Omega=-\left(\frac{\rho\varepsilon C_{\mathrm{F}}\sqrt{u^{2}+v^{2}}}{\sqrt{K}}\right)_{p}\Delta\Omega\cdot u_{p} \tag{24}$$

It is convenient to treat the Darcy and Forchheimer terms as source terms. However, Equations (23) and (24) indicate that, after integrating, both terms become a product of Darcy velocity component and a coefficient. The two coefficients can be added into the coefficients of the algebraic equation A_{p}^{u}, which will accelerate the convergence rate.

The procedure to obtain the pressure correction equation is also similar to that for homogenous fluid (Equation (20)), except for a small change

$$u_{\mathrm{e}}^{m}=\overline{(u^{m})_{\mathrm{e}}}-\Delta\Omega_{\mathrm{e}}\overline{\left(\frac{1}{A_{P}^{u}+\sum_{l}A_{l}^{u}}\right)_{\mathrm{e}}}\left[\left(\frac{\delta(\varepsilon p^{*})}{\delta x}\right)_{\mathrm{e}}-\overline{\left(\frac{\delta(\varepsilon p^{*})}{\delta x}\right)_{\mathrm{e}}}\right]^{m-1} \tag{25}$$

3.3. Interface treatment

In some cases, structured grids are difficult, even impossible, to construct for complex geometries. Therefore, in the present study, multi-block grids method is applied to provide a compromise

DOI: 10.1002/fld

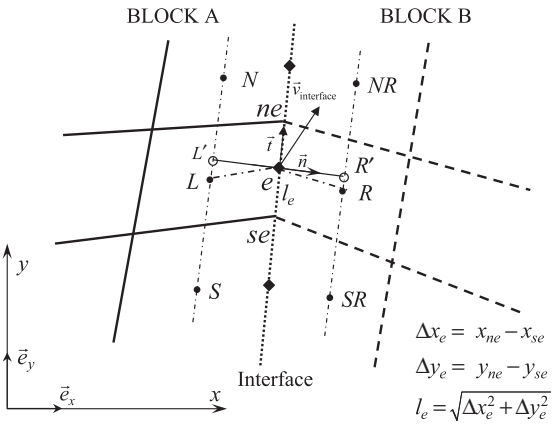

Figure 2. Interface between two blocks with matching grids.

between the simplicity and wide variety of solvers available for structured grids and ability to handle complex geometries that unstructured grids allow.

Figure 2 shows details of the interface between two different blocks. Two neighbouring control volumes, lying in Block A and Block B, respectively, share the interface. The grids in two neighbouring blocks match at the interface. Generally, there are three types of interfaces when the block-structured grids method is employed to calculate the flow in the composite region: fluid–fluid interface, porous medium–porous medium interface, and fluid–porous medium interface.

3.3.1. Interface between the same media. In this case, both blocks A and B (Figure 2) represent the same media, either fluid or porous. The method proposed by Lilek *et al.* [23] is applied to treat the block interface. A special data structure is designed to save the information at the interface, which consists of: the indices of the left (L) and right (R) neighbouring cells, the surface vector (pointing from L to R) and the coordinates of cell-surface centre (Figure 2). The interface cell surface shared by two CVs is treated as a cell surface in the interior of the block. Thus, the convective and diffusive terms at the block interface can be calculated in the same way as that (Section 3.1) for the cell faces in the interior of the block. Then the contributions from the interface cell faces, namely A_{L} and A_{R}, can be obtained.

Each interface cell face contributes to the source terms for the neighbouring CVs. Thus, if the east side of a CV is a block interface, the coefficient A_{E} (Equation (19)) is set to zero. However, the algebraic equation at node L receives the contribution $A_{\mathrm{R}}\varphi_{\mathrm{R}}$, while at node R, the contribution is $A_{\mathrm{L}}\varphi_{\mathrm{L}}$.

3.3.2. Interface between fluid and porous media. In this case, blocks A and B (Figure 2) represent fluid and porous medium, respectively. The velocity vector at the interface is given by $\mathbf{v}_{\text{interface}}$. It can be written in either the x–y or n–t coordinate system as

$$\mathbf{v}_{\text{interface}} = u\mathbf{e}_x + v\mathbf{e}_y = u_n\mathbf{n} + u_t\mathbf{t} \tag{26}$$

where u and v are the components of $\mathbf{v}_{\text{interface}}$ in the x and y directions while u_n and u_t are the $\mathbf{v}_{\text{interface}}$ components along n and t directions, respectively. And the component u_t then can be

DOI: 10.1002/fld

written as

$$u_t = u\mathbf{e}_x \cdot \mathbf{t} + v\mathbf{e}_y \cdot \mathbf{t} \tag{27}$$

By combining Equations (5), (7) and (26)

$$\frac{\mu}{\varepsilon}\left.\frac{\partial \mathbf{v}_{\text{interface}}}{\partial n}\right|_{\text{porous}} - \mu\left.\frac{\partial \mathbf{v}_{\text{interface}}}{\partial n}\right|_{\text{fluid}} = \beta\frac{\mu}{\sqrt{K}}u_t\mathbf{t} + \beta_1\rho u_t^2\mathbf{t} \tag{28}$$

The unit vector ($\mathbf{t}$) parallel to the interface (Figure 2) is calculated from

$$\mathbf{t} = \frac{(x_{\text{ne}} - x_{\text{se}})\mathbf{e}_x + (y_{\text{ne}} - y_{\text{se}})\mathbf{e}_y}{\sqrt{(x_{\text{ne}} - x_{\text{se}})^2 + (y_{\text{ne}} - y_{\text{se}})^2}} = \frac{\Delta x_{\text{e}}\mathbf{e}_x + \Delta y_{\text{e}}\mathbf{e}_y}{l_{\text{e}}} \tag{29}$$

By substituting the components of $\mathbf{v}_{\text{interface}}$ in the x and y directions, Equation (28) becomes

$$\frac{\mu}{\varepsilon}\left.\frac{\partial u}{\partial n}\right|_{\text{porous}} - \mu\left.\frac{\partial u}{\partial n}\right|_{\text{fluid}} = \beta\frac{\mu}{\sqrt{K}}\frac{u\Delta x_{\text{e}}\Delta x_{\text{e}} + v\Delta y_{\text{e}}\Delta x_{\text{e}}}{l_{\text{e}}^2} + \beta_1\rho\frac{\Delta x_{\text{e}}(u\Delta x_{\text{e}} + v\Delta y_{\text{e}})^2}{l_{\text{e}}^3} \tag{30}$$

$$\frac{\mu}{\varepsilon}\left.\frac{\partial v}{\partial n}\right|_{\text{porous}} - \mu\left.\frac{\partial v}{\partial n}\right|_{\text{fluid}} = \beta\frac{\mu}{\sqrt{K}}\frac{u\Delta x_{\text{e}}\Delta y_{\text{e}} + v\Delta y_{\text{e}}\Delta y_{\text{e}}}{l_{\text{e}}^2} + \beta_1\rho\frac{\Delta y_{\text{e}}(u\Delta x_{\text{e}} + v\Delta y_{\text{e}})^2}{l_{\text{e}}^3} \tag{31}$$

The derivatives at the interface are calculated from the values at auxiliary nodes L′ and R′; these nodes lie at the intersection of the cell face normal n and straight lines connecting nodes L and N or R and NR, respectively, as shown in Figure 2. The normal gradients at the interface can be calculated by using the first-order difference approximation

$$\left.\frac{\partial u}{\partial n}\right|_{\text{porous}} = \frac{u|_{\text{R}'} - u|_{\text{e}}}{L_{\text{eR}'}}, \quad \left.\frac{\partial v}{\partial n}\right|_{\text{porous}} = \frac{v|_{\text{R}'} - v|_{\text{e}}}{L_{\text{eR}'}} \tag{32}$$

$$\left.\frac{\partial v}{\partial n}\right|_{\text{fluid}} = \frac{v|_{\text{e}} - v|_{\text{L}'}}{L_{\text{L}'\text{e}}}, \quad \left.\frac{\partial v}{\partial n}\right|_{\text{fluid}} = \frac{v|_{\text{e}} - v|_{\text{L}'}}{L_{\text{L}'\text{e}}} \tag{33}$$

The Cartesian velocity components at L′ and R′ can be calculated by using bilinear interpolation or by using the gradient at the control volume centre

$$u|_{\text{L}'} = u|_{\text{L}} + (\text{grad}\, u)_{\text{L}} \cdot \mathbf{L}'\mathbf{L} \tag{34}$$

To obtain higher-order approximation of the derivatives, the velocity components at more auxiliary nodes may be needed. Alternatively, the shape functions may be used, which produces a kind of combined finite element/finite volume method for calculating the higher-order approximations.

By using Equations (30)–(34) and explicitly calculating the terms at the right-hand sides of Equations (30) and (31), the Cartesian velocity components u and v at the interface are obtained. Then the convective fluxes at the interface can be calculated. The diffusive fluxes are calculated from Equations (32) to (34). Then the coefficients A_{L} and A_{R} can be obtained.

To close the algebra equation system, the pressure at the interface must be determined. However, the pressure gradient at the interface may not be continuous due to the rather large Darcy and Forchheimer terms (Equation (4)), which may result in a rapid pressure drop at the porous side [15]. This discontinuity of the pressure gradient becomes more severe at higher Reynolds number

DOI: 10.1002/fld

and lower Darcy number. Thus, it requires special treatment to estimate the interface pressure from that of the vicinity at either side. A simplistic pressure estimation may give unrealistic, oscillatory velocity profile. The coupling issue of pressure–velocity at the interface was described in a recent paper by Betchen *et al.* [15] who proposed a solution that enables stable calculations. The pressure is extrapolated in the fluid side to a location at a small distance near the interface. From this location, a momentum balance is then used to estimate the interface pressure. This estimate is then averaged with the pressure extrapolated from the porous side to obtain the interface pressure. In the present paper, a less complex treatment was adopted. Extrapolations from the fluid and porous sides give two different estimates of the interface pressure. The average of the two estimates is used as the interface pressure. A small number of iterations is required for accuracy.

4. RESULTS AND DISCUSSION

4.1. Flow in a channel partially filled with a layer of a porous medium

The physical domain is shown schematically in Figure 3. It consists of a planar channel which is horizontally divided into a homogenous fluid region with height H_1 above and a fluid–saturated porous region with height H_2 below. The case of height ratio $H_2/H_1 = 1$ is considered.

The flow is assumed laminar and fully developed. The governing equations are simplified as follows:

$$\frac{\mathrm{d}^2 u}{\mathrm{d}y^2} = \frac{1}{\mu}\frac{\mathrm{d}p}{\mathrm{d}x} \quad \text{for the homogenous fluid} \tag{35}$$

$$\frac{\mathrm{d}}{\mathrm{d}y}\left(\frac{\mu}{\varepsilon}\frac{\mathrm{d}u}{\mathrm{d}y}\right) = \frac{1}{\varepsilon}\frac{\mathrm{d}(\varepsilon p_\mathrm{f})}{\mathrm{d}x} + \frac{\mu}{K}u + \frac{\rho C_\mathrm{F}}{\sqrt{K}}u^2 \quad \text{for porous medium region} \tag{36}$$

with introducing the dimensionless variables

$$U = \frac{\mu u}{G H_1^2} \quad \text{and} \quad Y = \frac{y}{H_1}$$

where

$$G = -\frac{\mathrm{d}p_\mathrm{f}}{\mathrm{d}x}$$

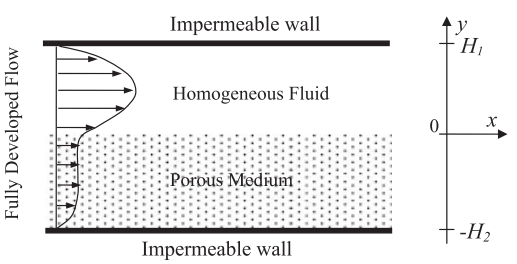

Figure 3. Schematic of flow in a channel partially filled with saturated porous medium.

DOI: 10.1002/fld

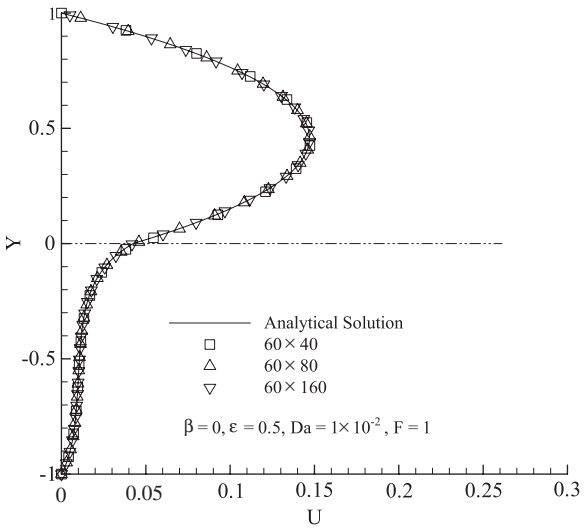

Figure 4. Effect of grid size on velocity profile.

Equations (35) and (36) can be rewritten as

$$\frac{\mathrm{d}^2U}{\mathrm{d}Y^2} = -1 \quad \text{for the homogenous fluid} \tag{37}$$

$$\frac{1}{\varepsilon}\frac{\mathrm{d}^2U}{\mathrm{d}Y^2} = -1 + \frac{1}{Da}U + FU^2 \quad \text{for porous medium region} \tag{38}$$

where Darcy number $Da = K/H_1^2$ and Forchheimer number $F = C_\mathrm{F}\rho G H_1^4/K^{\frac{1}{2}}\mu^2$. The boundary conditions are

$$U = 0 \quad \text{at } Y = 1 \quad \text{and} \quad U = 0 \; Y = -H_2/H_1 \tag{39}$$

$$\frac{1}{\varepsilon}\left.\frac{\mathrm{d}U}{\mathrm{d}Y}\right|_{\text{porous}} - \left.\frac{\mathrm{d}U}{\mathrm{d}Y}\right|_{\text{fluid}} = \frac{\beta}{\sqrt{Da}}U_{\text{interface}} \quad \text{at } Y = 0 \tag{40}$$

Following the proposal of Nield *et al.* [24], Equations (37)–(40) can be solved analytically as shown in Appendix A. Both numerical and analytical solutions are presented for validation of the present numerical implementation.

To ensure grid-independent solution and accurate resolution, a sufficiently fine mesh should be used. For the fully developed flow (Figure 3), a mesh of 60 grids in the x direction is found to be sufficient. In y direction, it is found that at least 40 grids are needed to obtain grid-independent solution (Figure 4), which is consistent with the results of Silva and de Lemos [3] and Costa *et al.* [4]. The interface velocities obtained with different grids are summarized in Table II. It confirms that above 40 grids in y direction there is little change in the results. Also, the interface velocity agrees with the analytical solution (of present study) to an accuracy of about 5%.

DOI: 10.1002/fld

Table II. Interface velocity with different grids in y direction.

Grids in y direction	Interface velocity
40	0.0444
80	0.0434
160	0.0428
Analytical solution	0.0423

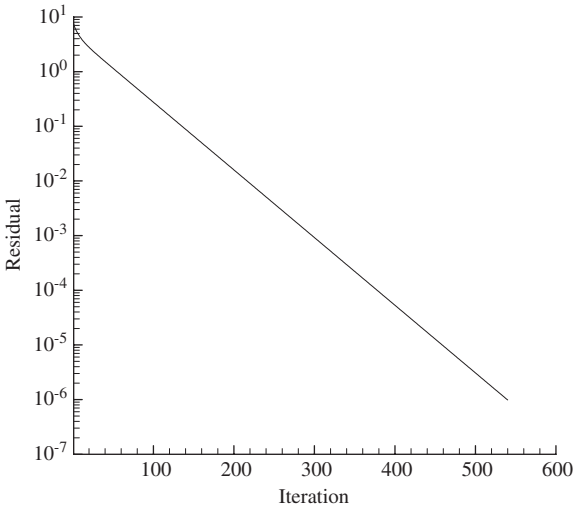

Figure 5. Variation of the residual as a function of iterations; 60×60 CVs grid.

Figure 5 shows the variation of the residual as a function of the number of the iterations. The rate of convergence is fast and the residual drops to 10^{-6} within 600 iteration steps when a mesh of 60×60 CVs is used.

Figure 6 shows the u velocity profile under different flow conditions. It is seen that the numerical and analytical results are in good agreement. The effect of the Darcy number (Da) on the u velocity profile is presented in Figure 6(a) in which the Da varies from 10^{-3} to 5×10^{-2} while the other parameters are kept constant. Although in practical applications, Da may not go up to 10^{-2} [25], nevertheless this range is also presented to show Da effect more clearly. From Figure 6(a), it is seen that the u velocity decreases with the increase in Da. When Da is less than 10^{-3}, the u velocity in the porous medium is almost zero, except the region near the interface. The effect of the porosity (ε) on the u profile is shown in Figure 6(b). The u velocity should decrease as the porosity decreases and the numerical and analytical results seem to show the trend. However, in the porous medium region around $-0.33 < Y < -0.62$, the u velocity is slightly larger when the porosity is smaller. This may be because the β chosen here is kept constant even though it should vary with the variation of ε. The Forchheimer number (F) does not have much effect on the velocity distribution. The velocity decreases slightly when F increases from 1 to 100 as shown

DOI: 10.1002/fld

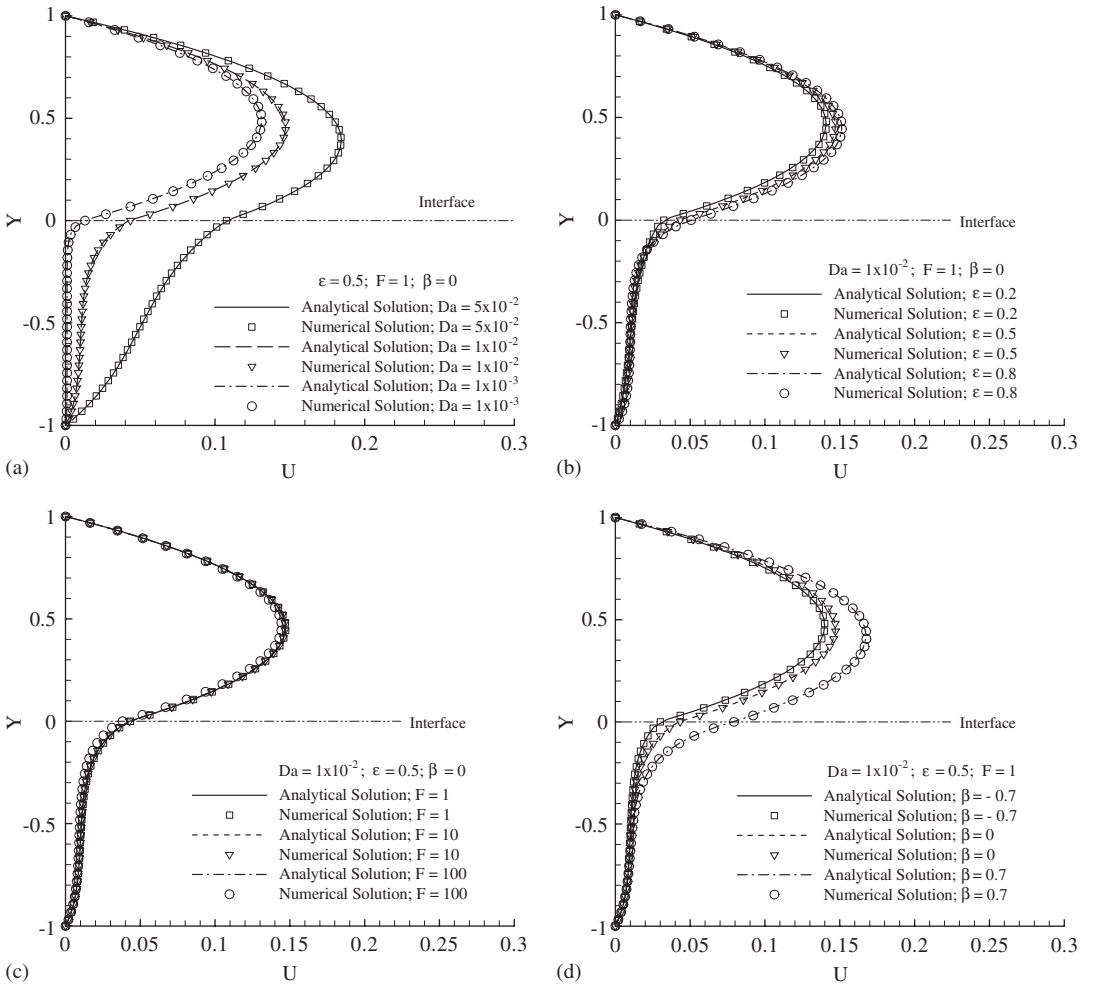

Figure 6. The u velocity profile under different flow conditions: (a) Darcy number effect; (b) porosity effect; (c) Forchheimer number effect; and (d) jump parameter effect.

in Figure 6(c). The effect of the jump parameter (β) on the flow is shown in Figure 6(d), which indicates that the u velocity increases noticeably as β increases.

4.2. Flow through a channel with a porous plug

The physical domain of the second problem is shown schematically in Figure 7, which is the same as that by Gartling *et al*. [14], Costa *et al*. [4] and Betchen *et al*. [15]. In this problem the flow passes through a planar channel with a porous plug under an imposed overall pressure gradient. Different from the first problem, the governing dimensionless parameters are: Reynolds number based on the mean velocity, $Re = \rho U H/\mu$, Darcy number $Da = K/H^2$, the porosity ε, Forchheimer coefficient C_F and jump parameters β and β_1. For this case, Forchheimer coefficient C_F is evaluated as $C_F = 1.75/\sqrt{150\varepsilon^5}$ [4, 15].

DOI: 10.1002/fld

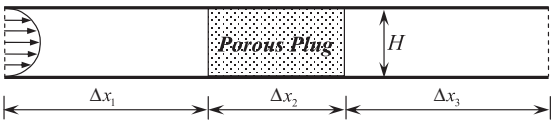

Figure 7. Schematic of flow in a channel with a porous plug.

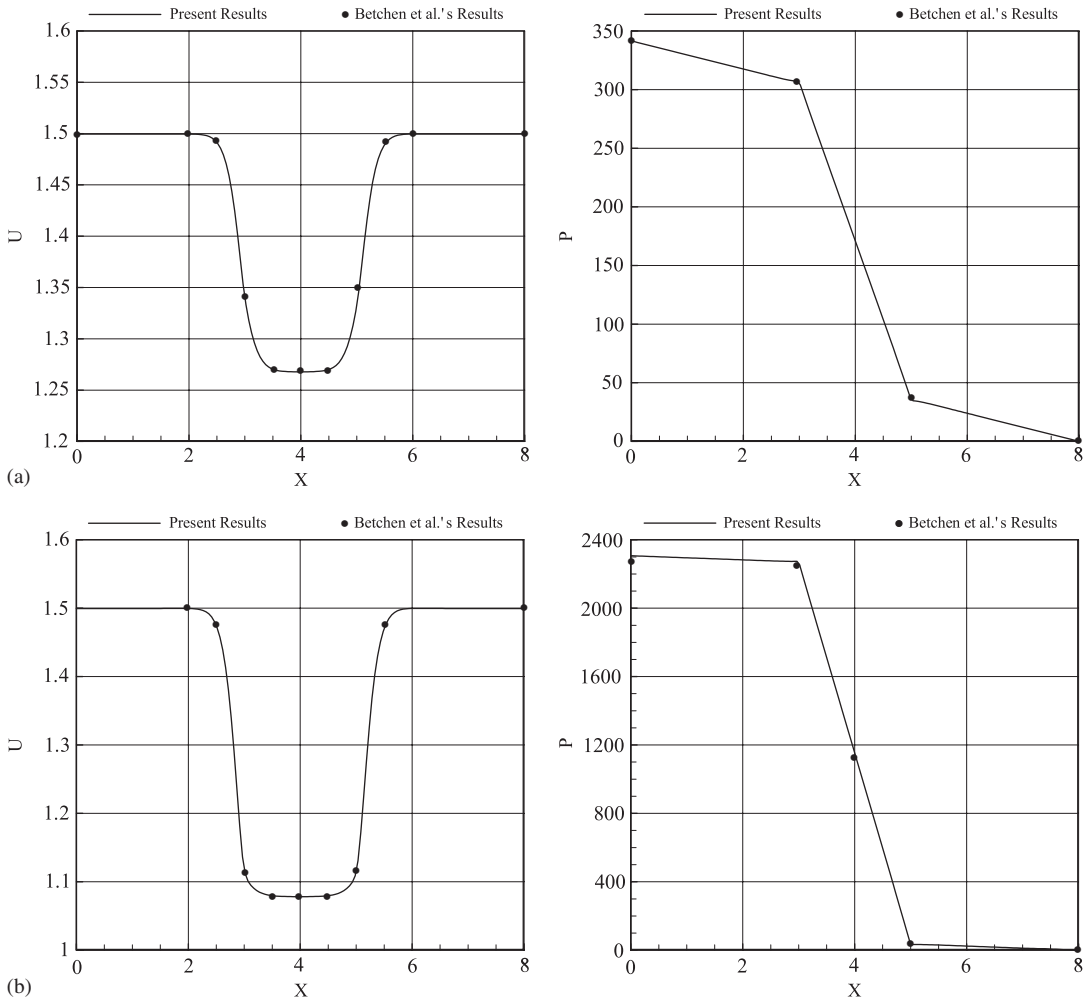

Figure 8. The velocity and pressure distributions along the centreline at: (a) $Da = 10^{-2}$ and (b) $Da = 10^{-3}$; other parameters are $Re = 1$, $\varepsilon = 0.7$, $\beta = 0$, $\beta_1 = 0$, $\Delta x_1 = \Delta x_3 = 3H$ and $\Delta x_2 = 2H$.

The numerical results for the case of $Da = 10^{-2}$ and 10^{-3} are shown in Figure 8, where the centreline u velocity and pressure along x direction are presented. The other parameters for the flows illustrated in Figure 8 are $Re = 1$, $\varepsilon = 0.7$, $\beta = 0$ and $\beta_1 = 0$. The lengths are set to $\Delta x_1 = \Delta x_3 = 3H$ and $\Delta x_2 = 2H$.

DOI: 10.1002/fld

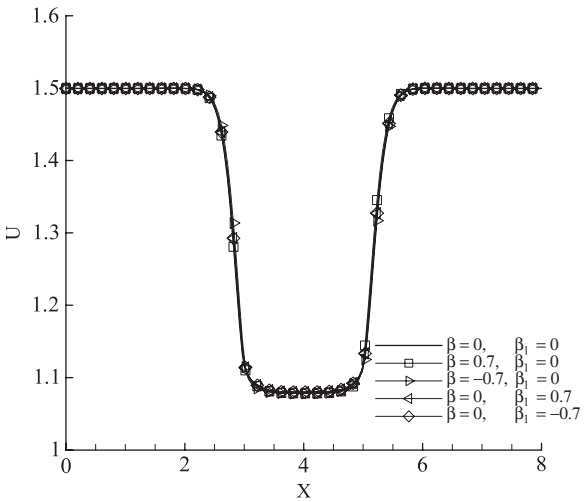

Figure 9. Effect of the jump coefficients on the velocity distribution along the centreline at $Da = 10^{-3}$, $Re = 1$, $\varepsilon = 0.7$, $\Delta x_1 = \Delta x_3 = 3H$ and $\Delta x_2 = 2H$.

The numerical studies by Costa *et al*. [4] and Betchen *et al*. [15] have shown that a mesh of $(20+20+20) \times 20$ CVs is fine enough to obtain accurate results; the node density in x direction is increasing towards the interfaces and the node distribution in y direction is uniform. In the present study, the same mesh was used and the preliminary numerical tests confirmed that the solutions are grid-independent.

Figure 8 shows that the velocity drops rapidly in the porous plug, across which there is a large pressure drop, especially for the case with the low Darcy number. The flow field is predominantly axial over most of the homogenous fluid and porous medium regions, but it is two-dimensional in the region near the interface between the homogenous fluid and the porous medium. The present results are in good agreement with those of Gartling *et al*. [14] and Betchen *et al*. [15]. The trends of the present results are in general agreement with that of Costa *et al*. [4] except for slight differences in the velocity magnitude in the porous medium.

The effect of the shear jump parameters β and β_1 on the centreline velocity distribution is shown in Figure 9. It is seen that the two parameters have very small effect as the dominant flow direction is perpendicular to the interface.

Another case similar to Betchen *et al*. [15] is investigated in which the Darcy number is set to $Da = 10^{-2}$ and the channel segment lengths (Figure 7) are: $\Delta x_1 = \Delta x_2 = 5H$ and $\Delta x_3 = 50H$. In this case (Figure 10), the shear jump coefficient also has a negligible effect on the velocity distribution along the centreline. The centreline velocity profile shows that the velocity remains free of oscillation in the region near the two interfaces; this indicates that the present method is capable of dealing with discontinuous pressure gradient at the interface.

Note that the present Reynolds number is limited to $Re = 200$ because above this value, velocity oscillation was observed. For higher Reynolds number, the Forchheimer term becomes dominantly large, which may cause severe pressure drop in the porous side. Thus, a severe discontinuity in pressure gradient arises at the interface and the difficulty in estimating the interface pressure may cause velocity oscillation there. The present method to estimate the interface pressure has been

DOI: 10.1002/fld

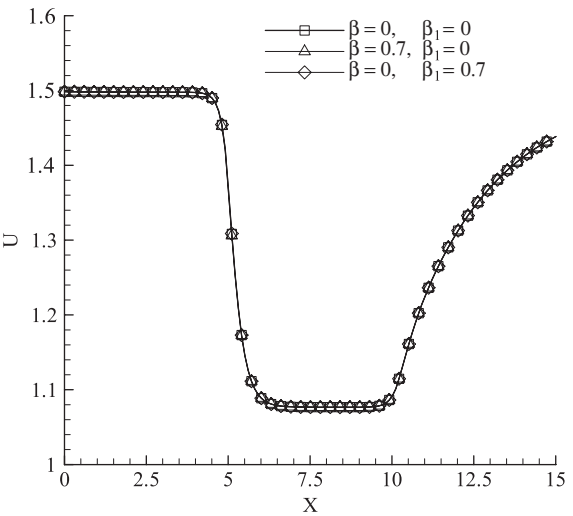

Figure 10. The velocity distribution along the centreline at $Da = 10^{-2}$, $Re = 200$, $\varepsilon = 0.7$, $\Delta x_1 = \Delta x_2 = 5H$ and $\Delta x_3 = 50H$.

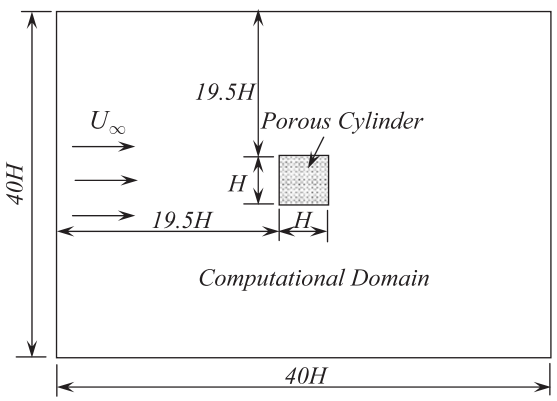

Figure 11. Schematic of flow past a porous square cylinder.

explained in Section 3.3. The more complex method to estimate the interface pressure proposed by Betchen *et al.* [15] is more robust for higher Reynolds number up to 1000.

4.3. Flow around a square porous cylinder

The above two problems concern internal flow problems with regions of a homogenous fluid and a porous medium. To illustrate an external flow problem with complex geometry, the flow around a square porous cylinder is considered. The computational domain is shown schematically in Figure 11. The governing dimensionless parameters are the same as those of the porous plug problem above: Reynolds number based on the mean velocity and the height of the cylinder,

DOI: 10.1002/fld

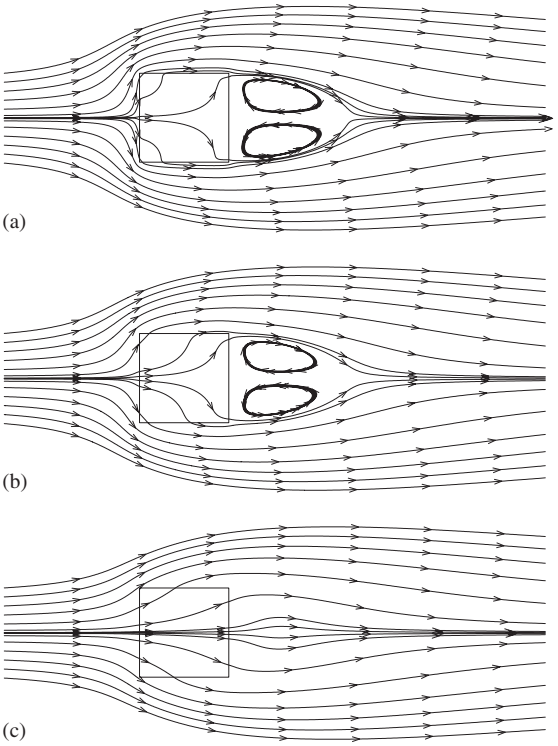

Figure 12. Streamlines of flow past a porous cylinder at different Darcy numbers: (a) $Da = 10^{-4}$; (b) $Da = 10^{-3}$; and (c) $Da = 10^{-2}$.

$Re = \rho U H/\mu$, Darcy number $Da = K/H^2$, the porosity ε, Forchheimer coefficient C_F and jump parameters β and β_1.

The flow streamline for the flow around a square porous cylinder at different Da are presented in Figure 12. In this case, Re is chosen as $Re = 20$ to ensure the steady and laminar flow. Three different $Da = 10^{-2}$, 10^{-3} and 10^{-4} are chosen and other parameters are kept constant namely, $\varepsilon = 0.4$, $C_F = 1$, $\beta = 0.7$ and $\beta_1 = 0$. The preliminary numerical test (data not shown) confirmed that a mesh of 40×40 CVs for the cylinder and a mesh of 160×100 CVs for the external region can provide grid-independent solutions. At smaller Da ($= 10^{-4}$ in Figure 12(a)), that is the cylinder permeability is small, very little fluid flows through the cylinder. Hence, the flow field resembles that around a solid cylinder. When Da increases to 10^{-3} (Figure 12(b)), the vortex in the wake is reduced as there is more bleed fluid. At higher Da ($= 10^{-2}$ in Figure 12(c)), the large bleed flow has prevented vortex formation.

Figure 13 shows the variation of recirculation length with the Darcy numbers, for $Re = 20$. The recirculation length is defined as the streamwise distance, along the wake centreline, from the cylinder rear to the re-attachment point. The recirculation length becomes longer with the decrease in the Darcy number. However, the recirculation length approaches to a constant value at low Darcy number as the porous cylinder tends to a solid one. The recirculation length at $Da = 10^{-7}$ is about 1.32 (Figure 13), which is rather close to the value of around 1.34 for the solid cylinder [26].

DOI: 10.1002/fld

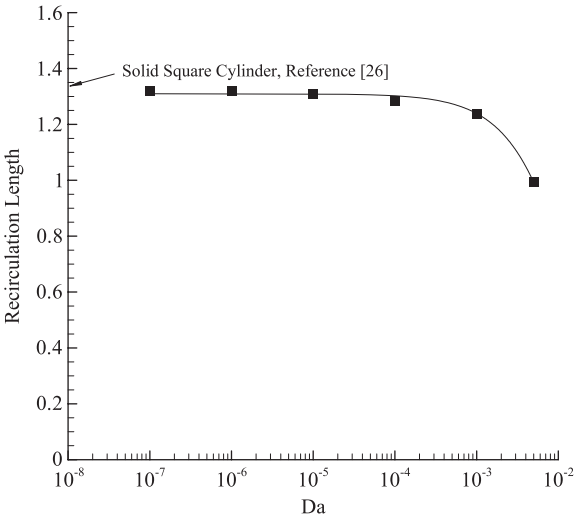

Figure 13. Variation of the recirculation length with the Darcy number.

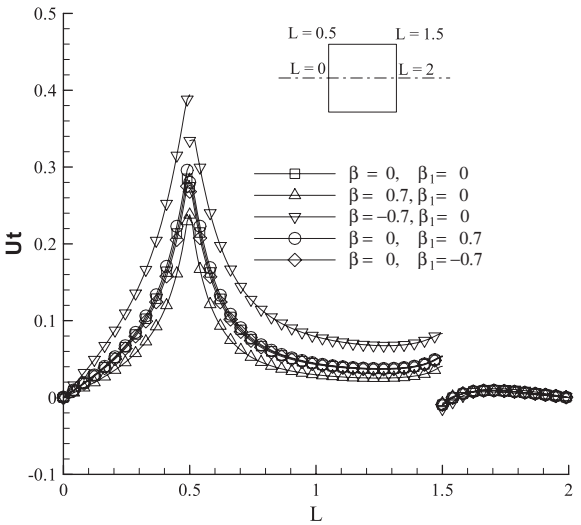

Figure 14. The tangential velocity distribution along the interface: $\varepsilon = 0.4$, $C_F = 1$, $Re = 20$ and $Da = 10^{-3}$.

Figure 14 shows the effects of the jump coefficients on the tangential velocity component at the porous–fluid interface. There is not much effect for the rear interface as the tangential velocity there is small. Elsewhere, the first coefficient β has a noticeable effect whereas the second coefficient β_1 has very small effect. From Equation (5), the viscous term $\beta(\mu/\sqrt{K})u_t$ is large if the permeability K is small, that is the Darcy number is small. The inertial term $\beta_1 \rho u_t^2$ may be important at high Reynolds number; however, the external flow would become unsteady, which is out of the scope of the present shear-jump modelling based on steady flow.

DOI: 10.1002/fld

5. CONCLUDING REMARKS

The main novelty of this paper is a numerical method for the theory developed by Ochoa-Tapia and Whitaker [15] to model the momentum jump condition at the boundary between a porous and fluid media, which includes both viscous and inertial jump parameters β and β_1. A distinctive feature of the present method is the use of multi-block grids which, together with body-fitted grids, makes it more suitable for handling complex geometries. The shear stress jump condition affects both the convective and diffusive fluxes. The normal stress condition, assumed continuous at the interface, is also needed in order to close the two sets of equations. The general method was applied to solve three flow configurations.

The numerical simulation of flow over a porous layer extends the work of Silva and de Lemos [3] by using multi-block grid and including the diffusive flux term; the results compares well with the analytical solution proposed by Nield *et al*. [24]. The numerical results for flow through a porous plug exhibit slight difference in velocity in the porous medium, as compared with the studies of Costa *et al*. [4]; however, there is good agreement with Gartling *et al*. [14] and Betchen *et al*. [15]. The centreline velocity profile is free of oscillation in the region near the two interfaces, which confirms that the present method is capable of dealing with discontinuous pressure gradient there. The numerical simulation of flow past a porous square cylinder demonstrates the use of multi-block grid for coupled fluid-porous flows involving complex geometries.

APPENDIX A

Integrating Equation (38) yields

$$\frac{1}{\varepsilon}\left(\frac{\mathrm{d}\langle U\rangle}{\mathrm{d}Y}\right)^2 = \frac{2}{3}F\langle U\rangle^3 + \frac{\langle U\rangle^2}{Da} - 2\langle U\rangle + C \tag{A1}$$

By using Equations (39) and (40), the constant C in Equation (A1) can be yielded

$$C = \varepsilon\left[\frac{\beta}{\sqrt{Da}}U_i + \left(\frac{1}{2} - U_i\right)\right]^2 - \left(\frac{2}{3}FU_i^3 + \frac{U_i^2}{Da} - 2U_i\right) \tag{A2}$$

Since $\mathrm{d}\langle U\rangle/\mathrm{d}Y$ should be real and negative at this region, we can obtain

$$\frac{\mathrm{d}\langle U\rangle}{\mathrm{d}Y} = -\sqrt{\varepsilon\left(\frac{2}{3}F\langle U\rangle^3 + \frac{\langle U\rangle^2}{Da} - 2\langle U\rangle + C\right)} \tag{A3}$$

Then we can integrate Equation (A3) to obtain

$$\int_0^{U_{\text{interface}}} Q(\langle U\rangle)\,\mathrm{d}\langle U\rangle = -\frac{H_2}{H_1} \tag{A4}$$

where

$$Q(\langle U\rangle) = -\left[\varepsilon\left(\frac{2}{3}F\langle U\rangle^3 + \frac{\langle U\rangle^2}{Da} - 2\langle U\rangle + C\right)\right]^{-1/2}$$

DOI: 10.1002/fld

In a similar fashion, we can obtain

$$\int_{\langle U\rangle}^{U_{\text{interface}}} Q(\langle U\rangle)\,\mathrm{d}\langle U\rangle = Y \tag{A5}$$

Given the values of Da, F and ε, the value of $U_{\text{interface}}$ is given in an inverse fashion by Equation (A4). Pairs of values (Y, U_i) determining the velocity profile can then be obtained from Equation (A5). Then the integrals in Equation (A4) can be solved using Romberg's numerical integration method.

REFERENCES

1. Mercier J, Weisman C, Firdaouss M, Quéré PL. Heat transfer associated to natural convection flow in a partly porous cavity. *Journal of Heat Transfer* (ASME) 2002; **124**:130–143.
2. Jue TC. Numerical analysis of vortex shedding behind a porous cylinder. *International Journal of Numerical Methods for Heat and Fluid Flow* 2004; **14**:649–663.
3. Silva RA, de Lemos MJS. Numerical analysis of the stress jump interface condition for laminar flow over a porous layer. *Numerical Heat Transfer A* 2003; **43**:603–617.
4. Costa VAF, Oliveira LA, Baliga BR, Sousa ACM. Simulation of coupled flows in adjacent porous and open domains using a control-volume finite-element method. *Numerical Heat Transfer A* 2004; **45**:675–697.
5. Goyeau B, Lhuillier D, Gobin D, Velarde MG. Momentum transport at a fluid–porous interface. *International Journal of Heat and Mass Transfer* 2003; **46**:4071–4081.
6. Nield DA. Discussion. *Journal of Heat Transfer* (ASME) 1997; **119**:193–194.
7. Beavers GS, Joseph DD. Boundary conditions at a natural permeable wall. *Journal of Fluid Mechanics* 1967; **30**:197–207.
8. Neale G, Nader W. Practical significance of Brinkman's extension of Darcy's law: coupled parallel flows within a channel and a bounding porous medium. *Canadian Journal of Chemical Engineering* 1974; **52**:475–478.
9. Vafai K, Kim SJ. Fluid mechanics of the interface region between a porous medium and a fluid layer–an exact solution. *International Journal of Heat and Fluid Flow* 1990; **11**:254–256.
10. Kim SJ, Choi CY. Convection heat transfer in porous and overlying layers heated from below. *International Journal of Heat and Mass Transfer* 1996; **39**:319–329.
11. Ochoa-Tapia JA, Whitaker S. Momentum transfer at the boundary between a porous medium and a homogeneous fluid I: theoretical development. *International Journal of Heat and Mass Transfer* 1995; **38**:2635–2646.
12. Ochoa-Tapia JA, Whitaker S. Momentum transfer at the boundary between a porous medium and a homogeneous fluid II: comparison with experiment. *International Journal of Heat and Mass Transfer* 1995; **38**:2647–2655.
13. Ochoa-Tapia JA, Whitaker S. Momentum jump condition at the boundary between a porous medium and a homogeneous fluid: inertial effect. *Journal of Porous Media* 1998; **1**:201–217.
14. Gartling DK, Hickox CE, Givler RC. Simulation of coupled viscous and porous flow problems. *Computational Fluid Dynamics* 1996; **7**:23–48.
15. Betchen L, Straatman AG, Thompson BE. A nonequilibrium finite-volume model for conjugate fluid/porous/solid domains. *Numerical Heat Transfer A* 2006; **49**:543–565.
16. Alazmi B, Vafai K. Analysis of fluid flow and heat transfer interfacial conditions between a porous medium and a fluid layer. *International Journal of Heat and Mass Transfer* 2001; **44**:1735–1749.
17. Hsu CT, Cheng P. Thermal dispersion in a porous medium. *International Journal of Heat and Mass Transfer* 1990; **33**:1587–1597.
18. Nithiarasu P, Seetharamu KN, Sundararajan T. Finite element modelling of flow, heat and mass transfer in fluid saturated porous media. *Archives of Computational Methods in Engineering* 2002; **9**:3–42.
19. Ferziger JH, Perić M. *Computational Methods for Fluid Dynamics* (2nd edn). Springer: Berlin, 1999; 222–233.
20. Muzaferija S. Adaptative finite volume method for flow predictions using unstructured meshes and multigrid approach. *Ph.D. Thesis*, University of London, 1994.
21. van Doormal JP, Raithby GD. Enhancements of the SIMPLE method for predicting incompressible fluid flows. *Numerical Heat Transfer* 1984; **7**:147–163.

DOI: 10.1002/fld

22. Rhie CM, Chow WL. Numerical study of the turbulent flow past an airfoil with trailing edge separation. *AAIA Journal* 1983; **21**:1525–1532.
23. Lilek Ž, Muzaferija S, Perić M, Seidl V. An implicit finite-volume method using nonmatching blocks of structured grid. *Numerical Heat Transfer B* 1997; **32**:385–401.
24. Nield DA, Junqueira SLM, Lage JL. Forced convection in a fluid-saturated porous-medium channel with isothermal or isoflux boundaries. *Journal of Fluid Mechanics* 1996; **322**:201–214.
25. Large JL. Effect of the convective inertia term on Bénard convection in a porous medium. *Numerical Heat Transfer A* 1992; **22**:469–485.
26. Sharma A, Eswaran V. Heat and fluid flow across a square cylinder in the two-dimensional laminar flow regime. *Numerical Heat Transfer A* 2004; **45**:247–269.

DOI: 10.1002/fld